The Role of Miscible Gas Mixing on CO_2-Enhanced Methane Recovery

Yamada, Kenta; Delshad, Mojdeh; Lake, Larry W.; Sepehrnoori, Kamy; Fernandes, Bruno Ramon Batista; Farajzadeh, Rouhi

DOI
10.2118/221024-MS

Publication date
2024

Document Version
Final published version

Published in
Society of Petroleum Engineers - SPE Annual Technical Conference and Exhibition, ATCE 2024

SPE-221024-MS

The Role of Miscible Gas Mixing on CO_2-Enhanced Methane Recovery

Kenta Yamada, Hilderbrand Department of Petroleum and Geosystems Engineering, The University of Texas at Austin, Austin, TX, United States ,now with ITOCHU Oil Exploration Co., Ltd.; Mojdeh Delshad, Larry W. Lake, and Kamy Sepehrnoori, Hilderbrand Department of Petroleum and Geosystems Engineering, The University of Texas at Austin, Austin, TX, United States; Bruno Ramon Batista Fernandes, Center for Subsurface Energy and the Environment, The University of Texas at Austin, Austin, TX, United States; Rouhi Farajzadeh, Faculty of Civil Engineering and Geosciences, Delft University of Technology University, Delft, the Netherlands / Shell Global Solutions International, The Hague, the Netherlands

 DOI 10.2118/221024-MS

This paper was prepared for presentation at the SPE Annual Technical Conference and Exhibition held in New Orleans, Louisiana, USA, 23 - 25 September 2024.

Abstract

Depleted gas reservoirs are viable choices for large-scale CO_2 storage and to displace remaining methane volumes to further increase the storage capacity (EGR). However, deployment of such projects depends on an informed knowledge of the magnitude of mixing of the miscible gases, efficiency in displacing in-situ methane by CO_2, composition of the produced gas, and CO_2 storage capacity. This study focuses on the fundamental analysis of mixing during CO_2-EGR using a numerical approach.

We propose to conduct very fine grid compositional simulations to provide insights into the mixing of CO_2 and methane in a gas reservoir at different reservoir and operational conditions. We first analyze a stratified layer model to understand the basic mechanisms of scale-dependency of dispersion and the significance of reservoir heterogeneity on fluid mixing. To consider more realistic reservoir heterogeneity, a two-dimensional stochastic reservoir model is analyzed to estimate dispersivity generated as fluids flow in porous media at different scales. Reservoir heterogeneity is represented by the Dykstra Parsons coefficient (V_{DP}) and autocorrelation length, and fluid properties are modeled depending on pressure and temperature conditions. Field-scale simulation is also performed to discuss the way dispersion is modeled in reservoir simulation affects simulated gas recovery.

Our study shows that the variance of permeability and convective spreading are the primary causes of fluid mixing at any scale. In addition, molecular diffusion is not always negligible in gas mixing even in large-scale heterogeneous reservoirs since gas has much larger diffusivity than liquid. Furthermore, the mechanism of fluid mixing during CO_2-EGR is complex with the interplay between convective spreading, transverse dispersion (including molecular diffusion), and gravity segregation. Although geoscientists often assume numerical dispersion can represent physical dispersion, our study indicates this is an oversimplification and could cause significant errors in calculated gas recovery. Permeability heterogeneity

is essential for the dispersion growth process and the final displacement behavior. Reservoir heterogeneity should be modeled with high-resolution grid models to analyze mixing behaviors more accurately.

Introduction

CO_2 Enhanced Gas Recovery (CO_2-EGR) could help sustain the energy supply in terms of improving natural gas recovery as well as CO_2 storage during the process. Although there have been limited field-scale applications (Van Der Meer et al., 2005; Pooladi-Darvish et al., 2008; CLEAN Partners et al., 2012), its great potential has encouraged researchers to perform extensive studies to analyze technical concerns and explore its feasibility (Liu et al., 2022; Wang et al., 2023).

Oldenburg et al. (2001; 2002) performed one of the first comprehensive field-scale feasibility studies for CO_2-EGR using reservoir simulation. Their simulation demonstrates that CO_2-EGR has excellent potential for gas recovery since the favorable mobility ratio between natural gas and injected CO_2 and gravity segregation support an ideal sweep with the limited impact of mixing between two fluids.

However, there are observations in the literature of early breakthrough of the injected CO_2 within one year (Vandeweijer et al., 2011) to three years (Pooladi-Darvish et al., 2008), and some cases resulted in early abandonment (Pooladi-Darvish et al., 2008) of field pilot projects. Reducing the CO_2 contamination in the produced gas is crucial for surface facilities, thus understanding the mixing between CO_2 and methane could be an essential driver to determine project life, total gas recovery, and CO_2 storage capacity.

Modeling field scale dispersive behavior is still controversial despite a long research history because of complicated mechanisms of how mixing is generated within the porous media and the inherence of numerical dispersion in reservoir simulation. Common practice is not modeling physical dispersion based on the assumption that numerical dispersion can represent the physical one. Oldenburg et al. (2001; 2002) use large grid size ($\Delta x=200m$) in their simulation to represent the expected longitudinal dispersion ($\alpha_L=100m$) in about 4,400 m well distance. Such a large dispersivity in the field scale has been recognized as scale-dependency of dispersivity.

Scale-dependency of dispersion creates confusion on the correct input value of dispersivity for field-scale reservoir simulation. Measured dispersivities from laboratory to field scale have been compiled by researchers over decades (Fig. 1). The relationship of measured longitudinal dispersivity to the scale of measurement shows a clear positive relation, providing evidence that large-scale has large dispersivity. It should be noted that the plots are in a log-log scale, and the data are highly scattered.

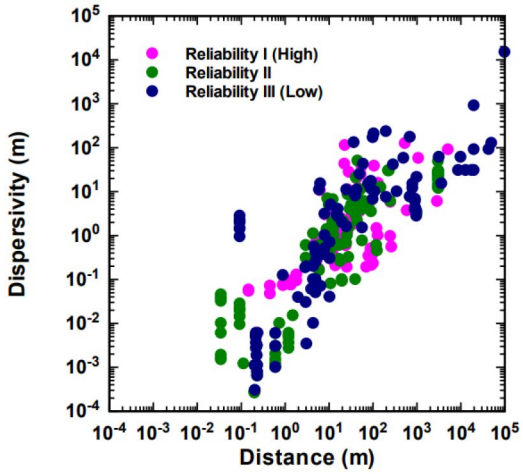

Figure 1—Dispersivity data measured over different length scales (Figure from John et al (2008), original data from Schulze-Makuch (2005), reliability indexes are defined by Gelhar et al. (1992), and data accumulated from numerous authors (Lallemand-Barres and Peauclecerf, 1978), etc.).

Considering the discussion above, how much physical dispersivity (α) should be input into field-scale reservoir simulation, although Oldenburg et al. (2001) modeled 100 m physical dispersivity by inherent numerical dispersion? Coats (2004) argued that we should input physical dispersivity on the order of 0.01 ft, not apparent dispersivities typically 100 to 1000 times larger than that. This is because apparent dispersivity is largely reflected by areal and vertical conformance, which results from well pattern, completion intervals, and heterogeneity. He also concluded that there is no scale dependence on physical dispersion.

Jha et al. (2009) cast double on Coats's standpoint, which is that dispersion results from convective spreading only. They used the concept of flow reversal (echo) and demonstrated that dispersion is a result of an interplay between convective spreading and diffusion. John et al. (2008) extended the theory from pore-scale to field-scale, concluding that dispersive mixing is significant in field-scale miscible displacement even in heterogeneous formation. Garmeh and Johns (2010) developed a response surface model based on reservoir simulation results to estimate local dispersivity.

Mixing within a gas phase has not been fully studied, past studies were focused on liquids (oil or water). Large (typically two orders of magnitude or more) molecular diffusivity and fluid compressibility in the gas phase may require a different explanation for the dispersive mechanism compared to the liquid phase. In addition, not only mixing but also overall displacement behavior during CO_2-EGR should be explored to optimize CO_2-EGR operation. Since CO_2 fluid properties vary significantly depending on pressure and temperature conditions relevant to EGR in depleted gas reservoirs, completely different development strategies may be required for each field.

The objective of this study is a fundamental understanding of the CO_2/methane mixing during CO_2-EGR, and resultant displacement behavior. To achieve this, we first perform dispersion analysis using numerical simulation to explore the mechanisms of how dispersion is generated in the porous media during gas displacement. Equal-density and equal-mobility fluids are used in the simulation to focus on pure dispersive behavior in heterogeneous media. Secondly, we perform numerical simulations for displacement analysis during CO_2-EGR. Not only dispersion but also gravity and mobility impacts are explored depending on different reservoir and operational conditions. We also compare simulation results by different modeling approaches of dispersion and show how they affect simulated gas recovery. We use a commercial software (CMG, 2023a) for the compositional reservoir simulations.

Methodology

Dispersion analysis

We first perform dispersion analysis using an analytical solution and numerical simulation for different reservoir heterogeneity at different scales. The objective is to estimate the apparent dispersivity generated as fluids flow in heterogeneous porous media. The main result from the simulation is the concentration profile over time. To focus on analyzing dispersive behavior, we convert the concentration profile to the equivalent dispersion coefficient and apparent dispersity by the following procedure.

Dispersivity estimation from mixing zone length. In an isothermal miscible displacement between two components in one-dimensional, homogeneous porous media, and assuming incompressible fluid, conservation of the displacing component can be described by the convection-dispersion equation (CDE). The dimensionless form of the equation is expressed by (Lake et al., 2014)

$$\frac{\partial C_D}{\partial t_D} + \frac{\partial C_D}{\partial x_D} - \frac{1}{N_{pe}} \frac{\partial^2 C_D}{\partial x_D^2} = 0 \tag{1}$$

where C_D is dimensionless concentration, t_D is pore volumes injected ($=vt/L$), x_D is dimensionless distance ($=x/L$), and N_{pe} is Peclet number ($=vL/K_L$). For continuous injection ($C_D\,(0,t_D)=1\ @t_D \geq 0$), the analytical solution is expressed by using the error function as

$$C_D = \frac{1}{2}\left[1 - \mathrm{erf}\left(\frac{x_D - t_D}{2\sqrt{\frac{t_D}{N_{pe}}}}\right)\right] + \frac{e^{x_D N_{pe}}}{2}\left[1 - \mathrm{erf}\left(\frac{x_D + t_D}{2\sqrt{\frac{t_D}{N_{pe}}}}\right)\right] \quad (2)$$

The dimensionless mixing zone, defined as the dimensionless distance between the position where $C_D=0.1$ and $C_D=0.9$, can be derived from equation (2) with neglecting the last term for simplicity since it generally has a small value as

$$\Delta x_D = \frac{x_{C_D=0.1} - x_{C_D=0.9}}{L} = 3.625\sqrt{\frac{t_D}{N_{pe}}} \quad (3)$$

In this study, dispersivity is estimated by using dimensionless mixing zone length from one-dimensional flow simulation results. We calculate the average concentration in the vertical direction to obtain the mixing zone length in the cross-sectionally averaged media (Fig. 2). Also, the location where the average concentration in the vertical direction is 0.5 is considered the mean travel distance.

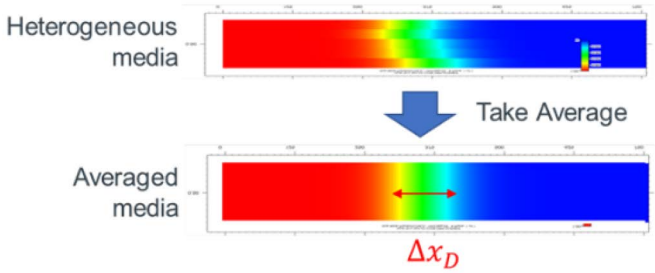

Figure 2—Schematic of estimating the mixing zone length of layered (heterogeneous) reservoir by taking an average concentration profile in each layer.

Equation (3) gives an equivalent Peclet number N_{pe} from the dimensionless mixing zone length, and the definition of the Peclet number $N_{pe}=vL/K_L$ gives an equivalent longitudinal dispersion coefficient K_L from N_{pe} .The resultant dispersion coefficient from numerical simulation includes three terms of molecular diffusion, physical dispersion, and numerical dispersion.

$$K_L = \frac{D_{mol}}{\tau} + \alpha_L |v| + D_{num} \quad (4)$$

where, D_{mol} is molecular diffusion coefficient, τ is tortuosity to consider actual diffusive travel distance in porous media (Perkins and Johnston, 1963), α_L is longitudinal dispersivity meaning the proportionality constant between velocity and physical dispersion coefficient, v is interstitial velocity, and D_{num} is numerical dispersion coefficient.

Therefore, the resultant longitudinal dispersivity α_L can be estimated by subtracting molecular diffusion and numerical dispersion terms from K_L and dividing by interstitial velocity. D_{num} is equated by the following equation when the difference equation is approximated with an implicit approach in time and upstream weighting is considered for the fluxes in X direction (Peaceman, 1977).

$$D_{num} = \frac{1}{2}v(\Delta x + v\Delta t) \quad (5)$$

Heterogeneous permeability field generation. A stochastic heterogeneous permeability field is used in our analysis. The models are generated by using three parameters: a Dykstra–Parson coefficient V_{DP}, a dimensionless autocorrelation length of permeability k_x for the flow direction λ_x, and a dimensionless autocorrelation for vertical direction λ_z. We use a commercial software (SLB-PETREL) to generate the 2-D permeability field.

The Dykstra–Parsons coefficient V_{DP} indicates the variance of permeability under the assumption that permeability data are drawn from a log-normal distribution, defined as

$$V_{DP} = \frac{k_{50} - k_{84.1}}{k_{50}} \tag{6}$$

where k_{50} is the log mean permeability and $k_{84.1}$ is one standard deviation below the mean. Typical petroleum reservoirs have a Dykstra–Parsons coefficient from 0.5 to 0.9 (Peters, 2012).

Spatial continuity is expressed by a semivariogram. The semivariogram is a function that shows the relationship between the semivariance γ of the distance between properties at two locations separated by a distance h and h as shown below.

$$\gamma(\vec{h}) = \frac{1}{2n}\sum_{i=1}^{n}\left[k_x(\vec{x}) - k_x(\vec{x}+\vec{h})\right]^2 \tag{7}$$

where x is location, n is the number of data pairs separated by the distance h. The autocorrelation length is the distance at which the semivariogram levels off in a semivariogram model. The dimensionless autocorrelation length is the autocorrelation length divided by the length of interest, usually the distance between the injection and the production points. A spherical semivariogram is used in this study.

Application for mixing in CO_2-EGR

We secondly analyze mixing during CO_2-EGR. The objective is to understand displacement behavior, including gravity segregation, channeling, and dispersion under the typical operational and reservoir conditions in the CO_2-Methane system. We also aim to explore the practical numerical modeling approach for field scale mixing during CO_2-EGR by comparing different approaches and resultant gas recovery.

Physical properties calculation. Pressure and temperature conditions are key factors determining fluid properties and resultant diffusive, gravitational, and mobility relations between injection and production fluid compositions. Since an isothermal condition is assumed, reservoir temperature refers to the initial reservoir temperature. On the other hand, reservoir pressure for CO_2-EGR varies depending on the operation; in other words, it depends on the timing of starting CO_2 injection after a certain level of reservoir depletion (primary production).

Fig. 3 shows the density difference between CO_2 and methane and the mobility ratio (inverse of viscosity ratio, μ_{CO_2}/μ_{CH_4}) in the range of pressure and temperature. Since the CO_2 critical point is close to operational temperature and pressure conditions where both properties vary near the critical point. At low pressure, the density difference is low, and the mobility ratio is close to (but less than) 1.0. As pressure increases, the density difference increases because CO_2 density increases faster, and the mobility ratio decreases further.

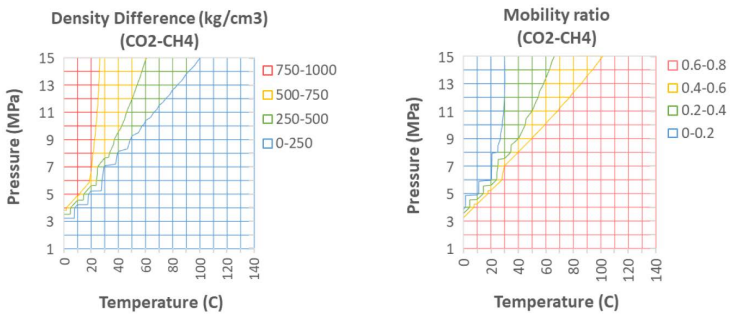

Figure 3—Density difference and mobility ratio between CO_2 and methane for various temperature and pressure (calculated using NIST chemistry webbook).

As for molecular diffusivity, the Sigmund model is used in this study to calculate the binary molecular diffusion coefficient accounting for pressure, temperature, and fluid compositions (Sigmund, 1976a, 1976b). The binary diffusion coefficient between components i and j in the gas phase mixture is

$$D_{ij} = \frac{\rho^0 D_{ij}^0}{\rho}\left(0.99589 + 0.096016 \quad \rho_r - 0.22035 \quad \rho_r^2 + 0.032874 \quad \rho_r^3\right) \tag{8}$$

where ρ is the molar density of the diffusing mixture at average mole fraction, and ρ_r is the reduced molar density calculated by

$$\rho_r = \rho\left(\frac{\sum_{i=i}^{n_c} y_i v_{ci}^{\frac{5}{3}}}{\sum_{i=i}^{n_c} y_i v_{ci}^{\frac{2}{3}}}\right) \tag{9}$$

where y_i is the molar fraction of component i in the gas phase, and v_{ci} is the molar volume of component i in the gas phase. $\rho^0 D_{ij}^0$ can be calculated by gas kinetics with Chapman-Enskog theory as follows (Bird et al., 2007),

$$\rho^0 D_{ij}^0 = 0.0018583\sqrt{T\left(\frac{1}{M_i} + \frac{1}{M_j}\right)}\frac{1}{\sigma_{ij}^2 \Omega_{ij} R} \tag{10}$$

where T is temperature, M_i is the molecular weight of component i, R is the universal gas constant, and σ_{ij} and Ω_{ij} are Lennard-Jones parameter and collision integral, respectively, between components i and j. Fig 4 shows the relationship between the binary molecular diffusion coefficient in the CO_2-Methane system calculated by Chapman-Enskog kinetic theory and pressure at a temperature of 60 °C. Pressure has a significant influence on the diffusion coefficient, which could reach 1.0×10^{-2} cm^2/s at low-pressures and is around 1,000 times larger in value than a typical value of brine-water at standard conditions.

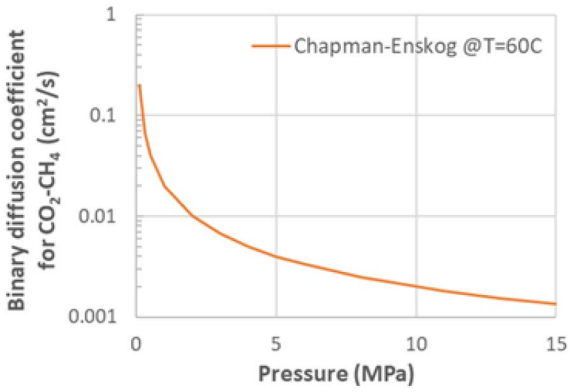

Figure 4—Binary molecular diffusion coefficient for CO_2- Methane system for different pressures.

The solubility of gas components in connate water is modeled using Henry's law. The fugacity of gaseous components i soluble in the aqueous phase is expressed by

$$f_{iw} = y_{iw} H_i \tag{11}$$

where y_{iw} is the mole fraction of component i. H_i is Henry's constant, which are the functions of pressure, temperature, and salinity as

$$\ln H_i = \ln H_i^* + \frac{\bar{v}_i(p - p^*)}{RT} \tag{12}$$

where H_i^* is Henry's constant at reference pressure p^* and temperature T, $\bar{v}_i$ is the partial molar volume of component i, p is pressure. In this study, Henry's constants are calculated using software (CMG, 2023b) using Li-Nghiem's method (Li and Nghiem, 1986).

Fundamental Analysis of Dispersion

Understanding scale-dependency of dispersion (Stratified layer model)

(i) No cross-flow case. We first analyze the relationship between reservoir heterogeneity and resultant dispersivity in field scale. The purpose is to validate whether inputting a large dispersivity observed in Fig. 1 into the simulation model is correct. We consider a heterogeneous reservoir model with stratified layers without vertical crossflow to represent heterogeneous channeling behavior.

We use an analytical solution of the Dispersion-Koval model developed by Naudomsup and Lake (2017). Their solution is for a one-dimensional convection-dispersion equation considering both local dispersion (represented by the Peclet numberN_{pe}) and heterogeneous channeling (represented by the Koval heterogenous factor H_K) for heterogeneous reservoir with stratified layer without vertical crossflow. The Koval heterogenous factor is practical in relating reservoir heterogeneity to vertical sweep efficiency compared to conventional heterogeneous parameters based on statistics. Paul et al. (1982) show the relationship between H_K and V_{DP} by the following equation.

$$\log(H_K) = \frac{V_{DP}}{(1 - V_{DP})^{0.2}}. \tag{13}$$

Using the analytical solutions by inputting N_{pe} andH_K, we calculate the effluent history by continuous tracer injection. Then the profile is fit by the Peclet number in an analytical solution for the conventional 1-D CDE by minimizing the root mean square error. The fitted Peclet number is converted to the resultant apparent dispersivity influenced by both local dispersion and heterogeneous channeling. We assume small local dispersion (N_{pe} = 1000), which is aligned with the bottom line of the historical measured data (Fig. 1) under the assumption that molecular diffusion is negligible ($N_{pe} \approx \alpha/L$ = 1000). We perform sensitivity to the Koval factor from 1 (homogeneous, which is equivalent to$V_{DP}=0$) to 7 (heterogeneous, which is equivalent to $V_{DP}=0.67$ by equation (13)) and analyze the resultant apparent dispersivity for different Koval factors.

Fig. 5 shows the resultant Peclet number and inverse for different reservoir heterogeneity (Koval factor). When H_k is 1, the outcome of N_{pe} is 1000, which is equivalent to the initial local dispersivity. However, when heterogeneity is present, the outcome of N_{pe} decreases significantly and the inverse ofN_{pe}, which is equivalent to dimensionless dispersivity (α/L), shows a steady increase along with the Koval factor. Compared to the input local dispersivity of $\alpha=0.001\ L$ and resultant dispersivity of $\alpha=120\ L$ at H_k =7, heterogeneous channeling seems to be quite dominant as apparent dispersivity, under the assumptions we made for this study.

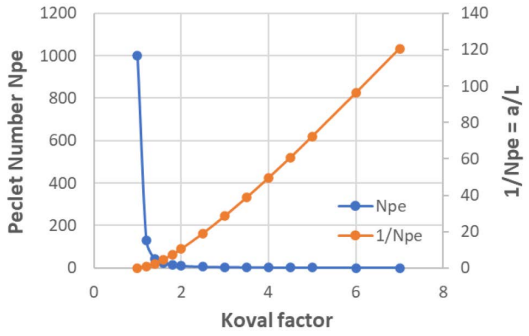

Figure 5—Estimated Peclet number with different Koval factors.

Fig. 6 shows the resultant dispersivity along with the scale for different Koval factors on the plot of measured data. A linear relationship exists between dispersivity and scale in the stratified layered flow without diffusive cross flow. Koval factors varying from 1 to 7 almost cover all scattered measured data in the plot. This result shows that heterogeneity is crucial for field-scale dispersivity. In other words, such a large dispersivity should not be input for reservoir simulation where heterogeneity is already represented by a geological model set; otherwise, the simulation overestimates fluid mixing.

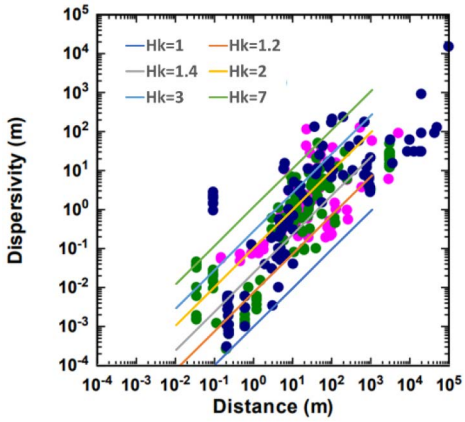

Figure 6—Estimated dispersivity along with distance for different Koval factors (adapted to the plot from John et al. (2008)).

(ii) With crossflow case. In real reservoirs, communication between layers plays an important role in field-scale dispersion. A sensitivity study with numerical simulation for a stratified layer model with diffusive crossflow is performed. The purpose is to analyze how dispersion grows where molecular diffusion occurs between layers. We prepare a unidirectional velocity field with 5 layers consisting of three high velocities and two low velocities, and the average velocity is V_o as shown in Fig. 7. Permeability varies with velocity variation at constant porosity and thickness for each layer. We perform sensitivity simulations for (1) heterogeneity (velocity variation), (2) average interstitial velocity, (3) thickness, and (4) molecular diffusion coefficient. The sensitivity parameters are summarized in Table 1. For simplicity, local dispersivity is neglected.

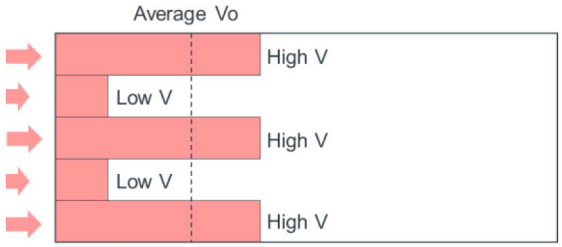

Figure 7—Schematic of the input velocity field in a 5-layer model.

Table 1—Sensitivity parameters for stratified layered simulation model.

Sensitivity parameters	Low	Base	High
Heterogeneity (Velocity Variation)	*high: 1.2 V_o low:0.7 V_o*	*high: 1.4 V_o low:0.4 V_o*	*high: 1.6 V_o low:0.1 V_o*
Average velocity V_o (m/d)	*0.1*	*1.0*	*10.0*
Total Thickness (m)	*0.316*	*1.0*	*3.162*
Molecular Diffusion Coefficient D_{mol} (cm^2/s)	1.0×10^{-5}	1.0×10^{-4}	1.0×10^{-3}

Fig. 8 shows the simulation results of the estimated dispersivity vs. mean travel distance for each sensitive simulation. Fig. 8a compares the results from the base case (using all base values of each sensitivity parameter) and the case with no diffusion. The no-diffusion case shows a linear relationship between dispersivity and travel distance, which aligns with the previous section's results. However, for the base case with molecular diffusion, it levels off when the travel distance arrives around 50 m, and finally, it reaches an asymptotic value. This explains that convective spreading (or heterogeneous channeling) is dominant when fluid starts to travel through heterogeneous formation, but later molecular diffusion works to equalize the concentration gradient between the layers, resulting in pure dispersive behavior.

Heterogeneity increases dispersivity by almost keeping the trend of the plots but shifting vertically in Fig. 8b. Heterogeneity mainly impacts convective spreading so that the large heterogeneity case shows a higher position in the plots, which is the same results in the previous section that a larger Koval factor results in a larger y-intersect in the plot but slope remains the same.

On the other hand, velocity, molecular diffusion coefficient, and thickness do not impact the linear section of convective spreading, but they affect the onset of the level-off, and that results in an asymptotic value of the final dispersivity (Fig. 8c, 8d, and 8e). Lake and Hirasaki (1981) introduced a dimensionless number, transverse dispersion number N_{TD}, based on the time required for fluid to cross the media in flow direction driven by convection (t_l) and in the transverse direction by diffusion or dispersion (t_t) in the two-layer porous media. v_{max} is the highest velocity in a layer, and $K_{T_{min}}$ is the transverse dispersion coefficient in the low-velocity layer. Assuming there is zero transverse physical dispersion $\left(K_{T_{min}} = D_{mol}/\tau\right)$ and using the average velocity for v_{max}, the equation can be simplified as

$$N_{TD} = \frac{t_l}{t_t} = \frac{L}{H^2}\frac{K_{T_{min}}}{v_{max}} \approx \frac{L}{H^2}\frac{D_{mol}/\tau}{v} \tag{14}$$

Fig. 8c, 8d, and 8e suggest that smaller transverse dispersion number N_{TD} takes more time to reach the asymptotic value, resulting in larger dispersivity. The resultant dispersivity increases with velocity and thickness, while it decreases with the molecular diffusion coefficient. In addition, the three figures for velocity, molecular diffusivity, and thickness are almost identical because the low and high values for these three sensitivity parameters have the same transverse dispersion number.

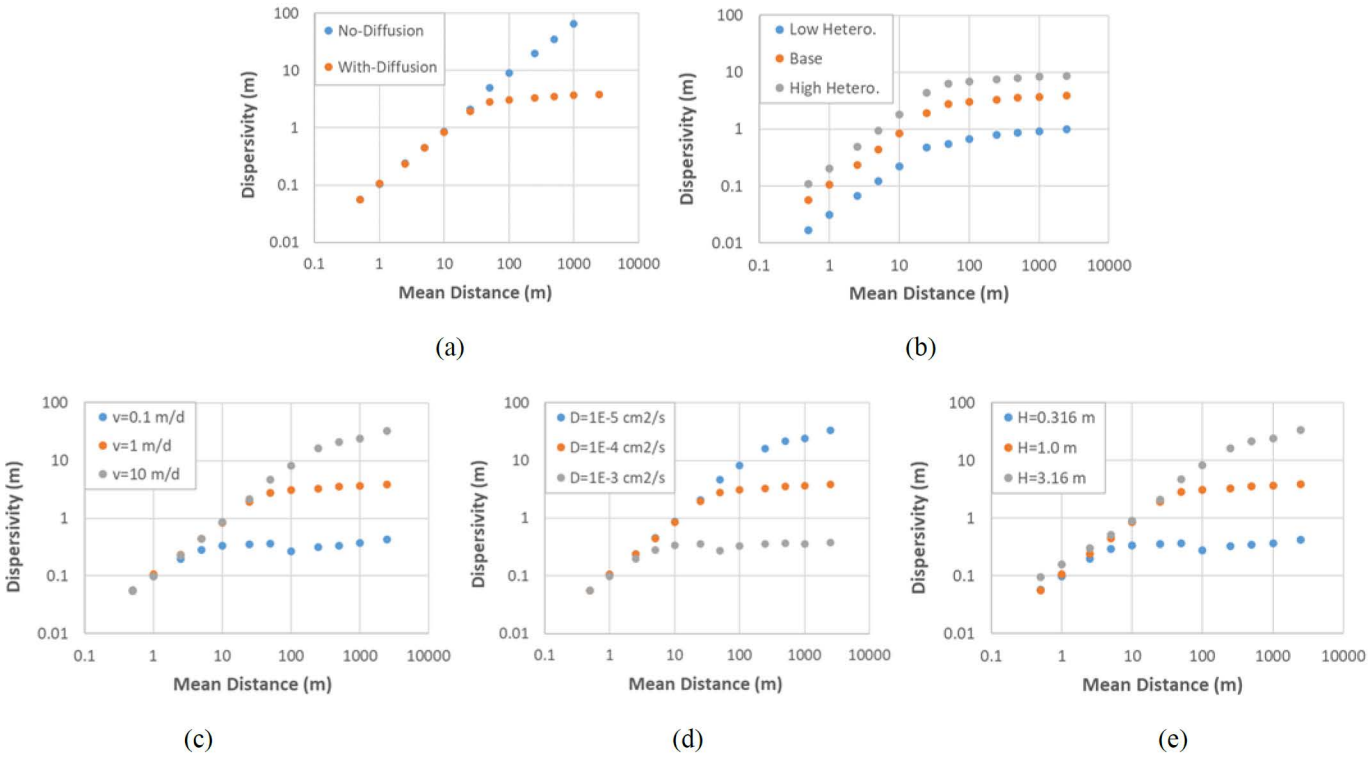

Figure 8—Estimated dispersivity vs. mean travel distance for (a) base case and the case without molecular diffusion, (b) different heterogeneity, (c) different velocity (v), (d) different molecular diffusion coefficient (D), (e) different thickness (H).

Although the transverse dispersion number N_{TD} is strictly for a two-layer medium, simulation results show that it can also capture the general behavior between convective spreading and dispersion in a simple stratified layer media such as the model used here.

Small-scale dispersion

Although the field-scale dispersion analysis discussed above implies that large dispersivity measured in Fig. 1 should not be input in the field-scale reservoir simulation, the question is how much dispersivity should be input. In this study, we apply the scaling-up approach performed by John (2008), in which dispersivity simulated in one grid-scale of a large-scale model is used as an input dispersivity for large-scale simulation.

To estimate apparent dispersivity in one grid-scale of the large-scale model, we perform reservoir simulation using a two-dimensional small-scale (1m×1m) model with a grid size of (1cm×1cm). We prepare a model with a distance five times larger than the region of study to remove the undesired boundary effect by a producer (Fig. 9). Heterogeneity is represented by permeability variation (Dykstra–Parsons coefficient V_{DP}), but with constant porosity. There is no autocorrelation length for the semivariogram (random distribution). We assume an isotropic permeability field with a mean value of 1000 mD. The model is initially saturated with pure methane with no mobile water saturation. A pseudo-component with the same properties as methane is injected from the model's left side by flow rate control to maintain the average interstitial velocity and produced from the right side by bottomhole pressure control. The initial reservoir pressure is set to 5MPa, and the temperature is 60 °C. We ignore physical dispersivity in this simulation. Tortuosity is assumed to be 1.4.

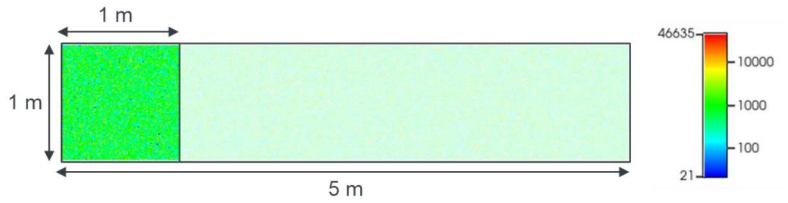

Figure 9—X-Permeability distribution (mD) of the 2-D small-scale model (V_{DP}=0.6).

Numerical sensitivity simulations are performed using different values for Dykstra–Parsons coefficient, average interstitial velocity, grid size, and molecular diffusion coefficient. Apparent dispersivity is calculated using mixing zone length from simulation results, which are explained in the methodology section. Fig. 10 shows the relationship between resultant K_L/D_{mol} and the local Peclet number P_e defined by vd_p/D_{mol}, where d_p is grain size. The plots show data collected by researchers from both lab experiments and simulation results, and the plot lines show simulation results from this work obtained by varying velocity for two heterogeneous models with V_{DP}= 0.6 and 0.9. The grid size is used corresponding to the grain size d_p for calculating the local Peclet number. Simulation results show good agreement with the collected data, and the variety of the collected plots stays within our simulation results at V_{DP}= 0.6 and 0.9. Fig. 10 explains that the local Peclet number P_e determines small-scale dispersive behaviors. A low local Peclet number (<0.1), such as low velocity, small grain size, or large molecular diffusivity, shows diffusion dominance. Convective dispersion starts to take place with increasingP_e, and at a certain point, it reaches a straight line for convective dominant dispersion.

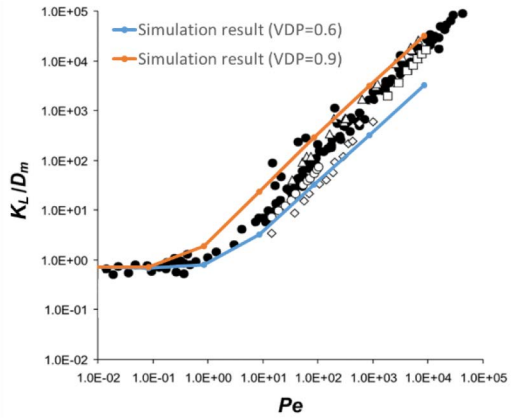

Figure 10—Comparison of the relationship between the ratio of dispersion coeff. (K_L) /molecular diffusion (D_m) and local Peclet number (P_e) from simulation results (plot line) with experimental data (plots) (adapted from Bijeljic et al. (2004). (Solid circles) experimental data using unconsolidated bead packs, (open circles, diamonds, and squares) from bead pack experiments obtained by magnetic resonance imaging, (triangles) bead pack experiments obtained by planar laser-induced fluorescence method).

Fig. 11 shows the estimated dispersivity at 1m travel distance vs. local Peclet number for two models with different permeability heterogeneities. The estimated dispersivity increases with the local Peclet number and reaches an asymptotic value at aroundP_e=*100*. The asymptotic value coincides with dispersivity in the case of no-molecular diffusion plotted by a dashed line. This means that molecular diffusion has a smaller impact at a larger local Peclet number, resulting in convective dispersion dominance. Also, heterogeneity has a significant influence on the resultant dispersivity, 0.28 cm for V_{dp}=*0.6* and 2.7 cm for V_{dp}=*0.6* corresponding to asymptotic values.

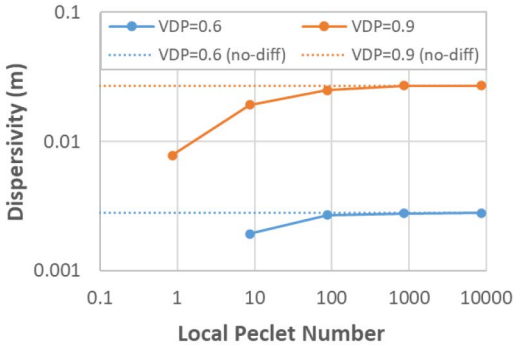

Figure 11—Estimated dispersivity at travel distance = 1m vs. local Peclet number with different V_{DP} values. Dashed lines refer to the cases without molecular diffusion and sold curves include molecular diffusion.

Most of the past research on small-scale dispersive behavior has been conducted by solving the Navier-Stokes equation with the convection-diffusion equation in porous structure or particle tracking simulation in porous networking model (Bruderer and Bernabé, 2001; Acharya et al., 2007; Jha et al., 2009). The results in this study show that finite volume-based compositional simulation with proper consideration of numerical dispersion can also model dispersive behavior at a small scale under the assumption that porous media consists of random packs of uniform-size grains.

Field-scale dispersion

We perform numerical simulations for a two-dimensional stochastic heterogeneous reservoir model to analyze large-scale dispersive fluid behavior in a field-scale reservoir (Fig. 12). The model is set to 200m×50m, considering the typical well distance in pattern floods, and the grid size is 1m×1m. We prepare a model with a five-times larger distance than our interest. Heterogeneity is represented by the Dykstra–Parsons coefficient ?sV_{DP}. Autocorrelation length for horizontal and vertical direction is set to $\lambda_x=0.6$ and $\lambda_z=0.1$. Reservoir conditions and settings in the simulation are the same as in the small-scale simulation. We assume a pure methane system, the flow rate is controlled by maintaining the average interstitial velocity of 1m/d, reservoir pressure is 5MPa, and temperature is 60 °C. kv/kh is 0.1, and tortuosity is assumed to be 1.4.

We perform sensitivity simulations for (1) Dykstra–Parsons coefficient, (2) molecular diffusion coefficient, and (3) input longitudinal dispersivity α_L. The molecular diffusion coefficient is varied from low as the typical value in the liquid phase to high for a gas phase. Input longitudinal dispersivity is set based on the results of dispersivity variation in small-scale simulation presented in the last section. Transverse dispersivity is set to a tenth of longitudinal dispersivity following a common practice (Perkins and Johnston, 1963). The parameters we use for the study are summarized in Table 2. Each simulation is performed by changing one parameter at a time and using the base case values for the other parameters.

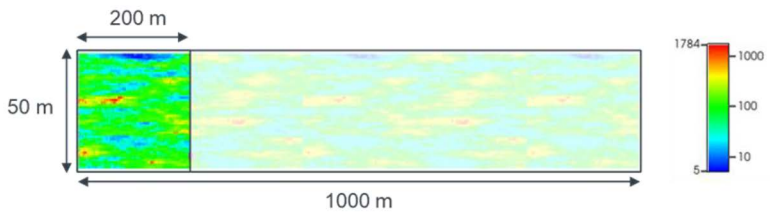

Figure 12—X-Permeability distribution (mD) of the 2-D large-scale reservoir model ($V_{DP}=0.6$).

Table 2—Sensitivity parameters for large-scale simulation.

Sensitivity parameters	Low	Base	High
Dykstra–Parsons coefficient, V_{DP}	*0.3*	*0.6*	*0.9*
Molecular diffusion coefficient, D_{mol} (cm²/s)	1.0×10^{-5}	1.0×10^{-4}	1.0×10^{-2}
Input longitudinal dispersivity, α_L (cm)	*0.3*	*1.0*	*10*

Fig. 13a shows the estimated dispersivity vs. mean distance for different heterogeneity. Dykstra–Parsons coefficient has a large impact on the resultant dispersive behavior. The estimated dispersivities when the fluid travels around 200m have considerable variation, 2.7m for $V_{DP}=0.3$ and 47.3 m for $V_{DP}=0.9$. Fig. 13b and 13c show the estimated dispersivity for different input molecular diffusion coefficients and longitudinal dispersivity. The figure implies that molecular diffusion and input local dispersivity have less impact on field-scale dispersion compared to the field-scale heterogeneous channeling in a heterogeneous reservoir with $V_{DP}=0.6$. However, the case with a large molecular diffusion coefficient ($D_{mol}=1\times10^{-2}\ cm^2/s$) seems to reduce the dispersivity. Therefore, even in the heterogeneous reservoir, molecular diffusion is not always negligible for gas displacement, and it can reduce the channeling effect.

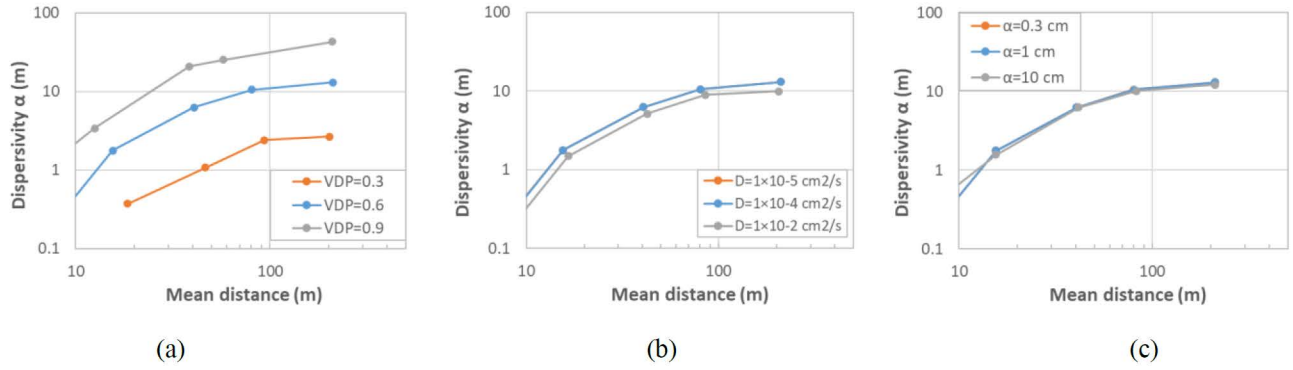

Figure 13—Estimated longitudinal dispersivity (α_L) vs. mean distance for (a) different heterogeneity (V_{DP}), (b) different molecular diffusion coeff. (D_{mol}), (c) different input local dispersivity (α).

Fig. 14 shows the estimated dispersivity including numerical dispersion for different grid sizes. Solid lines show calculated dispersivity without numerical dispersion. On the other hand, dotted lines show dispersivities with numerical ones. Numerical dispersivities calculated by equation (5) are about 0.5 m and 2.5 m when using 1m and 5 m grid blocks, respectively. Using a large grid size increases the overall dispersive behavior, but a low heterogeneous case ($V_{DP}=0.3$) is more sensitive to numerical dispersion than a highly heterogeneous case ($V_{DP}=0.9$) because the heterogeneous case already has large dispersion caused by channeling. A smaller grid is recommended for the less heterogeneous cases than the heterogeneous cases to accurately represent the real dispersivity.

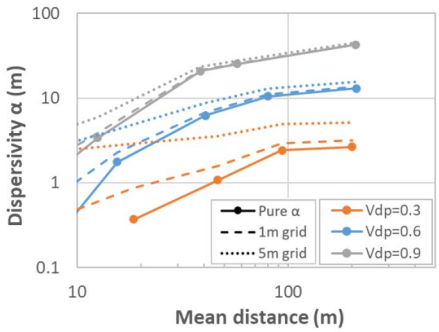

Figure 14—Estimated dispersivity including numerical dispersion for different grid sizes.

Mixing in CO_2-Enhanced Gas Recovery

How reservoir and operational conditions impact displacement in CO_2-EGR

In the fundamental dispersion analysis, we analyzed only dispersive behaviors using equal-density and equal-mobility fluids. In this section, we first perform a sensitivity simulation for CO_2-EGR using a two-dimensional stochastic heterogeneous reservoir. The objective here is to understand the general flow behavior, including gravity segregation, channeling, and dispersion under the typical operational and reservoir conditions in the CO_2-methane system.

This study assumes a single-phase flow in which CO2 and methane are completely miscible. This is a fair assumption at pressure and temperature conditions relevant to CO2-EGR (Hughes et al., 2012). Also, pure CO2 and pure methane are assumed as injectant and in situ gas, respectively, and assume isothermal reservoir temperature at 60 °C.

Fig. 15 shows the schematic of the model. The model is set to 200m×50m with a grid size of 1m×1m. Heterogeneity is represented by Dykstra–Parsons coefficient $V_{DP}=0.6$, and the dimensionless autocorrelation length λ for x and z directions are 0.6 and 0.1, respectively. Pure methane is saturated at initial conditions, and pure CO_2 is injected for gas recovery. Input longitudinal and transverse dispersivity are 1cm and 0.1 cm, respectively. Molecular diffusivity is modeled using the Sigmund model, but CO_2 and methane solubility in brine are not modeled. Sensitivity simulations are performed for reservoir pressure, fluid interstitial velocity, x-direction permeability, and kv/kh ratio. Each simulation is performed by changing one parameter at a time and using the base case values for the other parameters. The base values and their ranges are summarized in Table 3.

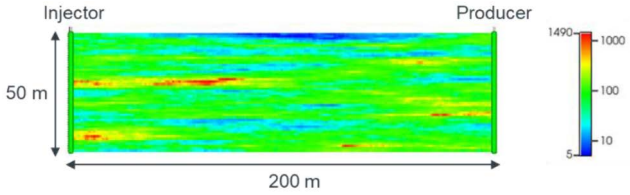

Figure 15—2-D heterogeneous reservoir model (X-permeability field, mD).

Table 3—Sensitivity parameters for CO2-EGR simulation.

Sensitivity parameters	Low	Base	High
Reservoir pressure (MPa)	1	5	15
Average interstitial velocity (m/d)	0.1	1.0	10.0
x-direction permeability k_x (mD)	10	100	1000
Vertical to horizontal peremability ratio, k_v/k_h	0.01	0.1	1.0

Reservoir pressure determines mobility, gravity segregation, and diffusive properties. CO_2-EGR always has favorable mobility conditions, so the impact of mobility ratio is negligible, but density difference and molecular diffusivity vary significantly in the pressure range associated with CO_2-EGR (Fig. 3 and Fig. 4).

Fig. 16 shows the injected CO_2 concentration profile after 0.4 pore volume injected for different reservoir pressures. Overall, channeling behavior exists since the reservoir is heterogeneous ($V_{dp}=0.6$). In the case of low reservoir pressure at 1MPa, the channeling behavior is reduced, and a more diffusive concentration profile is observed. This is caused by the larger molecular diffusion at low-pressure conditions for the gas phase. In contrast, when the reservoir pressure is 15MPa, the gravity segregation is more pronounced. CO_2 has a liquid-like density under this pressure range with a higher contrast in density between the two gases leading to gravity segregation against in situ methane.

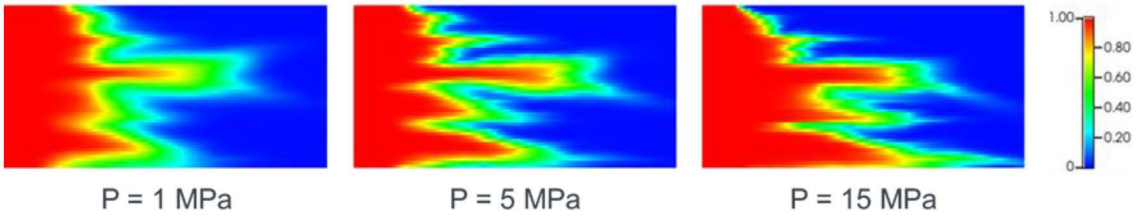

Figure 16—CO_2 mole concentration profiles at PVI=0.4 for different reservoir pressures.

Fig. 17 shows the CO_2 mole concentration profile for each sensitivity parameter at PVI=0.4. Channeling is dominant for most of the cases, but in the cases of high permeability and low velocity, gravity segregation is dominant, and their behaviors are similar since these two cases have similar gravity numbers $N_g = k_x \Delta\rho g / (\mu_o u_T)$ (Gharbi et al., 1998). In addition, if we compare these two cases, the case with low velocity has less channeling since low-velocity increases transverse dispersive behavior and works to equalize the concentration gradient among the layers, as discussed previously. Also, high kv/kh introduces gravity segregation since it increases the effective aspect ratio $\left(R_L = (L/H)\sqrt{k_z/k_x}\right)$. The effective aspect ratio is a key parameter to determine Vertical Equilibrium (VE) (Shook et al., 1993). In summary, permeability channeling is often dominant in heterogeneous reservoirs. However, reservoir and operational conditions can also change the flow behavior. Dimensionless scaling groups are still insightful for basic understanding even for heterogeneous media.

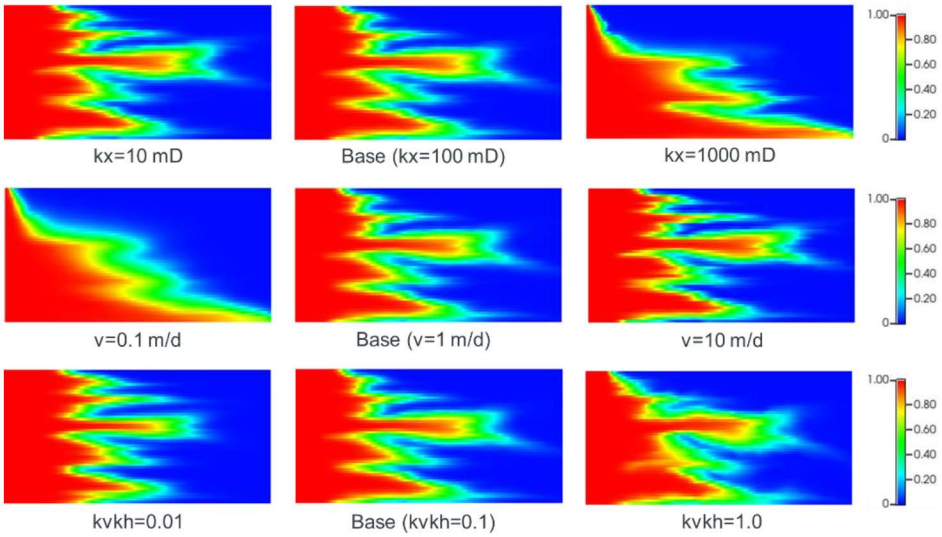

Figure 17—CO_2 mole concentration profiles at PVI=0.4 for sensitivity simulations. (top) profiles with different horizontal permeabilities (middle) profiles with different interstitial velocities, (bottom) profiles for different kv/kh.

Two-dimensional field scale simulation

The second study performs a field-scale two-dimensional reservoir simulation based on a depleted gas field. The objective is to show how the methodology to model dispersion affects simulated gas recovery. We follow Oldenburg's previous work (Oldenburg et al., 2001). They analyzed the feasibility of CO_2-EGR for a gas field in California that showed great potential for CO_2-EGR with limited gas mixing.

A homogeneous reservoir simulation model was developed similar to the one in Oldenburg et al. The reservoir has a 1 km width with vertical dimensions of 100 m and a horizontal extent of 6600 m with 0.78 degrees of dip angle. The model has 660 gridblocks (33×20) with a grid size of 200m×5m (Fig. 18). Primary production was performed from 1936 by a producer at the top of the reservoir. Then CO_2 injection was followed from 1999 by an injector located at 2000 m from the flank. Their simulation was performed using the TOUGH2 reservoir simulator with the EOS7C module to simulate gas and water flow in natural gas reservoirs. The simulations in this paper use a compositional reservoir simulator CMG-GEM with molecular diffusivity and solubility options. Only CO_2 solubility in brine is considered in our study. Table 4 summarizes the model properties. Some properties and production data from the paper are unavailable; hence, we use reasonable values for the input parameters. The pore volume is also adjusted so that the calculated production, pressure, and produced composition profiles match the results from Oldenburg et al.

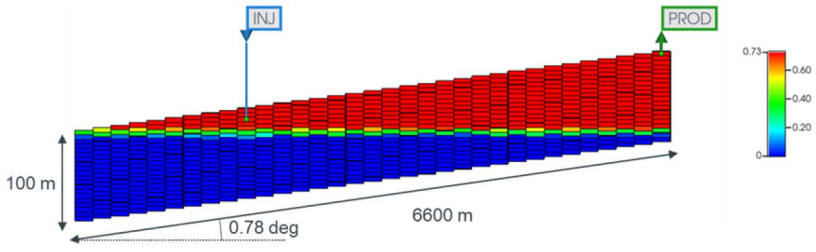

Figure 18—Reservoir model with initial gas saturation (original coarse grid model).

Table 4—Properties used in two-dimensional field scale simulation.

Properties	Value
Initial reservoir pressure (MPa)	12.6
Reservoir temperature (°C)	65
Porosity	0.35
k_x (mD)	1000
kv/kh	0.01
Capillary pressure	van Genuchten model $\left(m = 0.2,\quad S_{lr} = 0.27,\quad 1/\alpha = 8.4 \times 10^{-4}(Pa),\quad P_{capmax} = -10^5(Pa),\quad S_{ls} = 1.0\right)$
Relative permeability	Gas: Corey model (S_{gr}=*0.01*), Liquid: van Genuchten model
Molecular diffusion	Sigmund model, τ=*1.4*
CO_2 solubility	Henry's model (Henry's constants are calculated by Li-Nghiem's method assuming salinity =*100,000 ppm*)

It is a common practice that numerical dispersion is regarded as physical dispersion. Oldenburg's study used large grids with 200 m length in the flow direction for their simulation to represent 100 m dispersivity (Oldenburg et al., 2001) when the time step is small enough. This large dispersivity seems reasonable as a proxy for apparent dispersivity, considering a large well distance of 4,600 m. However, as we discussed before, this measured dispersivity is the consequence of the combined effect of convective spreading by heterogeneity and dispersive mixing. Therefore, we implement reservoir heterogeneity with fine grid blocks to see how the way dispersivity is modeled impacts gas recovery.

The new fine-grid model has 22,000 gridblocks (1,100×20) with a grid size of 6m×5m in x and z directions, respectively. The expected numerical dispersivity is around 3m, which is much less than the one from the original coarse grid model. The fine-grid model minimizes numerical dispersion and captures more realistic physical behavior. We prepare four fine-grid reservoir models with different reservoir heterogeneity. The first model is homogeneous, and the other three models have stochastic heterogeneous permeability fields with different Dykstra–Parsons coefficients (V_{DP}=*0.6,0.7,0.8*). They have the same autocorrelation lengths (λ_x=*0.6*,λ_z=*0.1*) and are generated by the same seed numbers to remove the influence of undesired randomness from the realizations. We input 10 cm of longitudinal dispersivity and 1cm of transverse dispersivity to consider the expected apparent dispersivity on a grid scale (6m).

Fig. 19a shows methane mass production. Since the producer is controlled at a constant flow rate, the rate is constant initially; then it declines along with CO_2 production. Fig. 19b shows the CO_2 mass fraction profile after starting CO_2 injection. Heterogeneity significantly impacts the timing of CO_2 breakthrough at the producer. In addition, the profile from the original coarse grid model is quite similar to the result from a fine-grid heterogeneous model with a Dykstra–Parsons coefficient of 0.7. This means the way to model dispersivity using a large grid block (and resultant numerical dispersivity) somehow represents dispersive behavior with reservoir heterogeneity.

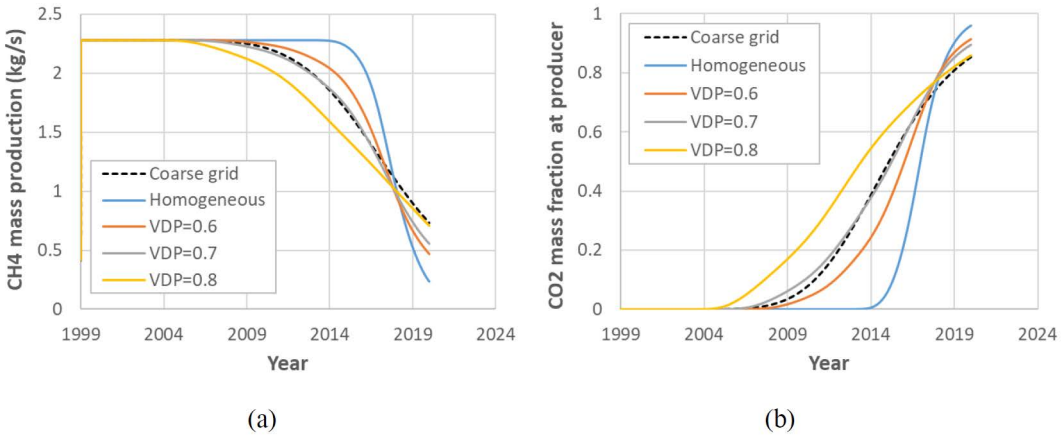

(a) (b)

Figure 19—(a) Methane mass production rate and (b) CO_2 mass fraction at producer during CO_2 injection for different models.

Fig. 20 shows the CO_2 concentration at different times for the coarse-grid homogeneous and fine-grid heterogeneous models with a Dykstra–Parsons coefficient of 0.7. In the coarse grid model, a uniform mixing zone is developed by numerical dispersion. In the heterogeneous model, however, the process of creating a mixing zone is complex. The injected CO_2 experiences convective spreading (channeling) by flowing in a heterogeneous permeability field. The combination with other effects, such as transverse dispersion (including molecular diffusion) and gravity segregation, determines the final shape of mixing zones. Therefore, the consequences are similar, but the physical mechanisms are different.

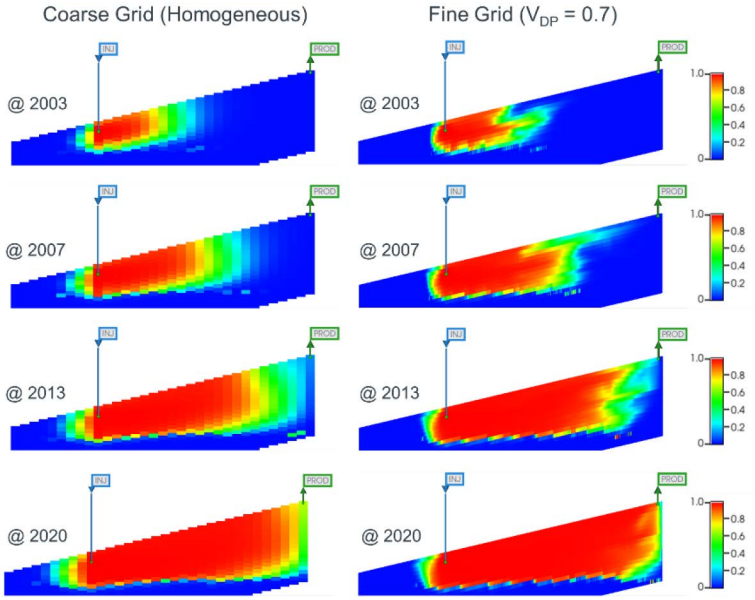

Figure 20—CO_2 concentration (mole fraction) at different times for (left) homogeneous coarse grid model, and (right) fine grid model with Dykstra–Parsons coefficient of 0.7.

The coarse grid model could miss important physical phenomena and lead to a poor estimation of gas recovery. Fig. 21 shows comparisons between simulation results from the coarse-grid model and fine-grid heterogeneous model ($V_{DP}=0.7$) for different reservoir properties. Fig. 21a shows a comparison between larger input transverse dispersivity ($\alpha_T=20cm$) and the original value ($\alpha_T=1cm$). The left figures show that the heterogeneous model has a smaller mixing zone because large transverse dispersion works to reduce the channeling effect. On the other hand, the coarse-grid homogeneous model cannot represent these interplays between channeling and transverse dispersion (or molecular diffusion). As a result, the heterogeneous model

causes CO_2 breakthroughs several years later than the case with small transverse dispersion, while the coarse grid model does not make a difference, as shown in the right figure. Fig. 21b shows a comparison between smaller horizontal permeability (k_x=*100mD*) and the original value (k_x=*1,000mD*). As discussed previously, small horizontal permeability mitigates gravity segregation, and convection becomes more dominant. Therefore, the heterogeneous model shows a significant channeling effect (left figure), which results in an early breakthrough by several years (right figure). However, the coarse grid model cannot capture these phenomena.

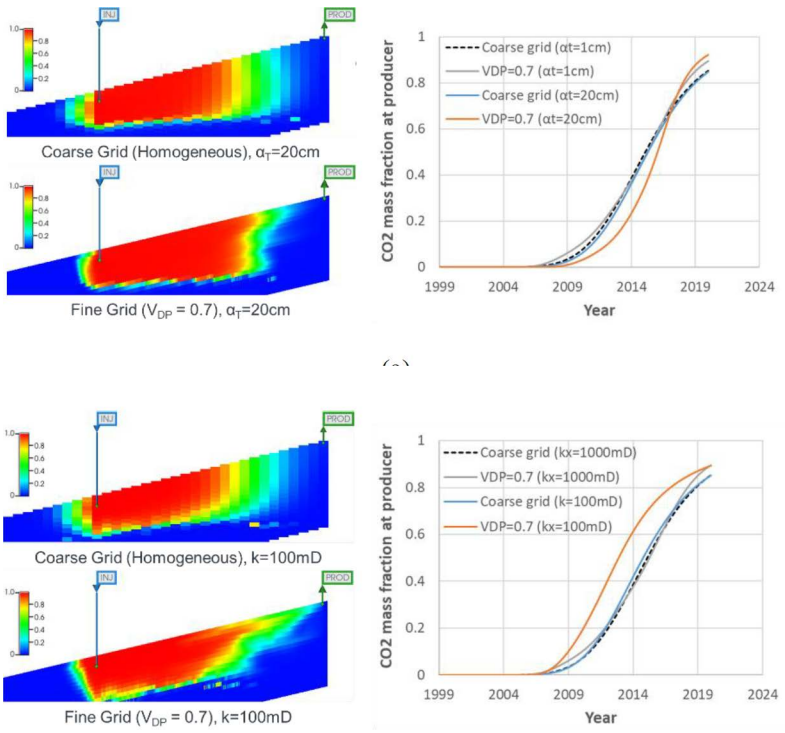

(b)

Figure 21—Comparison of simulation results from the homogeneous coarse-grid and heterogeneous fine-grid models for (a) different input transverse dispersivity (b) different horizontal permeability. Left figures show CO_2 mole concentration map in 2010, and right figure shows mass fraction of CO_2 at the producer.

In summary, modeling dispersivity using a large grid block (and the resultant numerical dispersivity) approximately represents dispersive behavior similar to that of a heterogeneous reservoir. However, this simple model cannot capture the physical interplays behind the dispersion and could lead to inaccurate computed gas recoveries and methane purities. Reservoir heterogeneity should be modeled with fine grids to analyze mixing behavior more accurately.

Three-dimensional five-spot pattern field scale simulation

To extend the discussion to more realistic reservoir conditions, three-dimensional reservoir simulations were modeled. Fig. 22 shows the simulation model of one-quarter of the five-spot well pattern. The model has 200m in the horizontal direction, and the thickness is 50m, assuming the symmetry element of a 40-acre 5-spot pattern where CO_2 is injected at the center well, and methane is produced by surrounding wells. It has 250,000 gridblocks (100×100×25) with fine grid sizes of 2m×2m×2m. Three reservoir models with different stochastic heterogeneous permeability fields (V_{DP} =0.3, 0.6, and 0.8) are generated. These models have the same autocorrelation lengths, which are 120m and 5 m in the horizontal and vertical direction, respectively. Other basic properties of the simulation are in Table 5.

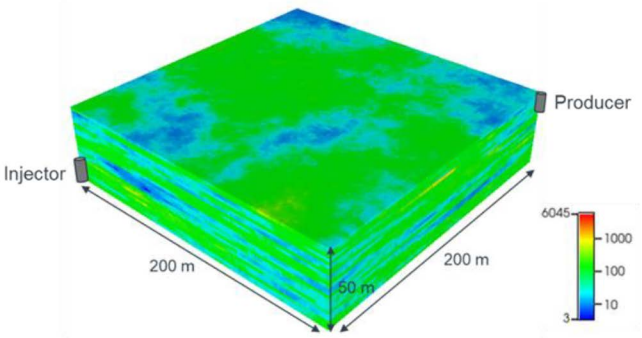

Figure 22—Three-dimensional reservoir simulation model of one-quarter of the five-spot well pattern. The color bar shows a horizontal (isotropic in x and y) permeability field (mD) for the heterogeneous model with a Dykstra–Parsons coefficient of 0.6.

Table 5—Properties used in three-dimensional field scale simulation (five-spot pattern case).

Properties	Value
Initial reservoir pressure (MPa)	5
Reservoir temperature (°C)	60
Porosity	0.3
Mean k_x (mD)	100
kv/kh	0.1
Input physical dispersivity	Longitudinal dispersivity α_L=*10 cm* Transverse dispersivity α_T=*1 cm*
Molecular diffusion	Sigmund model τ=1.4
CO_2 solubility	Henry's model (Henry's constants are calculated by Li-Nghiem's method assuming salinity =*100,000 ppm*)

The CO_2 injector and the producer are perforated at the bottom and the top of the reservoir, respectively, to utilize the benefit of gravity segregation. The wells are controlled by flow rate and reservoir pressure is almost constant. We perform simulations with two different flow rate conditions with different reservoir heterogeneities to demonstrate the interplay of gravity and channeling in a five-spot flood pattern. The high flow rate condition is that CO_2 is injected at the constant mass rate of 1.0 kg/s, and reservoir fluids are produced at a constant flow rate equivalent to 0.3 kg/s methane production, while the low flow rate case is one-fifth of those of the high flow rate.

Fig. 23 and Fig. 24 show the mass fraction of produced CO_2 and the CO_2 concentration in the cross-section between injector and producer at PVI=0.21, respectively, for different heterogeneous models. The left figures are for a high flow rate (convection dominant), while the right figures are for a low flow rate (gravity dominant). Gravity segregation is decreased in high flow rate conditions, and convection is more dominant. Therefore, the timing of CO_2 breakthroughs is largely impacted by reservoir heterogeneity. On the other hand, in low flow rate conditions, the gravitational effect is dominant even though there is high reservoir heterogeneity. This is why reservoir heterogeneity has a minor impact on CO_2 purity compared to the convection-dominant situation.

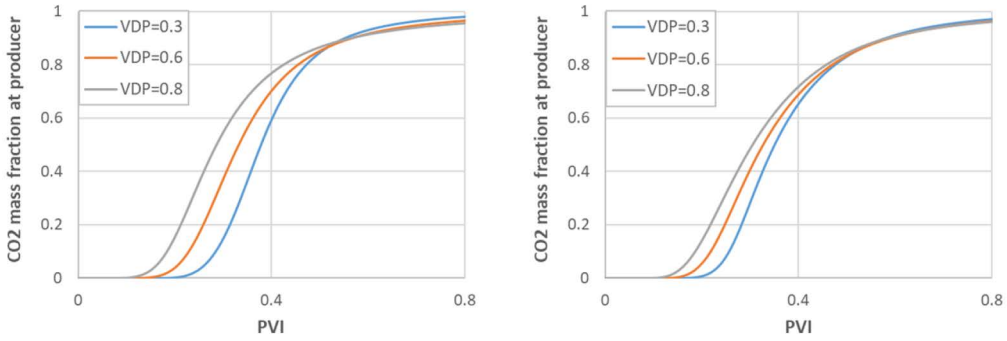

Figure 23—Mass fraction of produced CO_2 for different heterogeneous models (left) high flow rate case, (right) low flow rate case (keeping the total mass of injected CO_2 was constant).

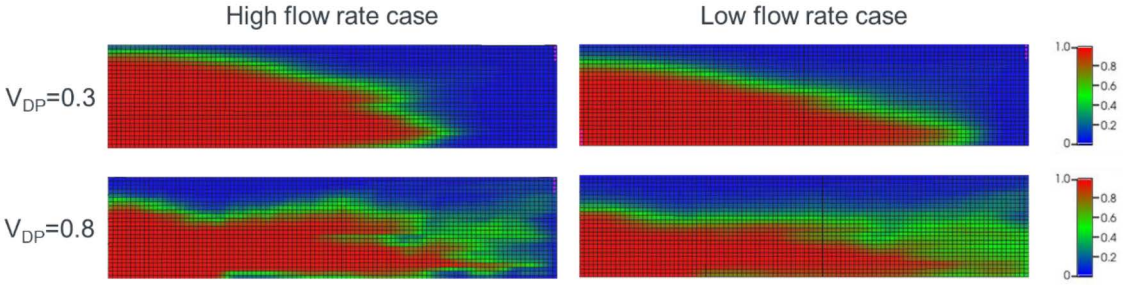

Figure 24—CO_2 concentration (mole fraction) in the cross-section between injector and producer for different reservoir heterogeneous models (V_{DP}=0.3 and 0.8) at PVI=0.21 (left) high flow rate case (right) low flow rate case.

Another finding is that the preferable displacement is different for different reservoir heterogeneity. A highly heterogeneous reservoir with for example a Dykstra–Parsons coefficient of 0.8 is more favorable to sweep using gravity segregation while minimizing channeling. On the other hand, in the less heterogeneous or homogeneous reservoir, convective-dominated displacement is favorable to minimize early breakthrough by underrunning gravity tongue.

Conclusions

This study analyzes the mixing of CO_2 and methane during CO_2 Enhanced Gas Recovery (EGR) and the resultant displacement behavior. We perform (1) dispersion analysis using an analytical model and numerical simulation to explore the mechanisms of how dispersion is generated inside porous media and (2) numerical simulations for CO_2-EGR to consider not only dispersion but also how the changes in gravity and mobility impact displacement behavior at different reservoir and operational conditions. Key insights observed in this study are:

- Heterogeneity (the variance of x-permeability) and resultant convective spreading are the primary causes of apparent dispersivity at any scale. Along with fluid traveling, they also induce the scale-dependency of dispersivity. Molecular diffusion generally reduces convective spreading, and dispersivity can reach an asymptotic value when certain conditions are satisfied. Local Peclet number and Transverse dispersion number are helpful for qualitative understanding of these behaviors at small-scale and large-scale models, respectively.
- In a large-scale heterogeneous reservoir with V_{DP} of 0.6, convective spreading (channeling) is dominant and unaffected by molecular diffusion and input physical dispersion. However, molecular diffusivity has a wide variation in the gas phase depending on pressure conditions and cannot always be negligible during gas displacement. In large-scale reservoir simulation, a smaller grid size is recommended as reservoir heterogeneity decreases to accurately model real dispersivity.

- Pressure and temperature conditions are key factors in determining fluid properties and resultant diffusive, gravitational, and mobility impact on displacement performance. More attention should be paid to reservoir pressure since it varies depending on the timing of starting CO_2-EGR. Mobility ratio is always favorable in CO_2- Methane displacement, so its impact is negligible, but density difference and molecular diffusivity vary significantly in the pressure range associated with CO_2-EGR. Low reservoir pressure conditions tend to introduce diffusive fluid behavior, but high reservoir pressure can promote gravity segregation.
- Reservoir Modelers sometimes simplify the impact of dispersion using a large grid size (and the resultant numerical dispersion) in field-scale reservoir simulation. We confirmed that the large grid size model does show a similar recovery profile to a realistic heterogeneous reservoir model. However, the physics behind the flow behavior are different. The mixing zone is impacted by the combination of heterogeneous channeling, transverse dispersion (including molecular diffusion), gravity effect, etc. Just using a coarse grid model with numerical dispersion could overestimate or underestimate gas recoveries. Heterogeneity should be modeled correctly with fine grids to analyze the mixing behavior accurately.
- The 2D cases were extended to 3D heterogeneous models for five-spot well pattern flooding. In general, gravity segregation is believed to be a good mechanism for CO_2-EGR, but our study implies that the favorable displacement process is different depending on reservoir heterogeneity.

Acknowledgment

The authors acknowledge Shell Global Solutions International, Petroleum Development Oman for supporting this research. The authors also thank the Computer Modeling Group and SLB for providing access to their software. Kenta Yamada would like to acknowledge ITOCHU Oil Exploration Co., Ltd. Authors acknowledge Shell Global Solutions International for their permission to publish this work.

References

Bijeljic, B., Muggeridge, A.H., Blunt, M.J., 2004. Pore#scale modeling of longitudinal dispersion. *Water Resources Research* **40**, 2004WR003567. https://doi.org/10.1029/2004WR003567

Bird, R.B., Stewart, W.E., Lightfoot, E.N., 2007. Transport phenomena, Revised ed. ed. Wiley, New York.

CLEAN Partners, Kühn, M., Tesmer, M., Pilz, P., Meyer, R., Reinicke, K., Förster, A., Kolditz, O., Schäfer, D., 2012. CLEAN: project overview on CO2 large-scale enhanced gas recovery in the Altmark natural gas field (Germany). *Environ Earth Sci* **67**, 311–321. https://doi.org/10.1007/s12665-012-1714-z

CMG, 2023a. GEM User Guide.

CMG, 2023b. WINPROP User Guide.

Coats, K.H., Whitson, C.H., Thomas, L.K., 2004. Modeling Conformance as Dispersion, in: All Days. Presented at the SPE Annual Technical Conference and Exhibition, SPE, Houston, Texas, p. SPE-90390-MS. https://doi.org/10.2118/90390-MS

Garmeh, G., Johns, R.T., 2010. Upscaling of Miscible Floods in Heterogeneous Reservoirs Considering Reservoir Mixing. *SPE Reservoir Evaluation & Engineering* **13**, 747–763. https://doi.org/10.2118/124000-PA

Gelhar, L.W., Welty, C., Rehfeldt, K.R., 1992. A critical review of data on field#scale dispersion in aquifers. *Water Resources Research* **28**, 1955–1974. https://doi.org/10.1029/92WR00607

Gharbi, R., Peters, E., Elkamel, A., 1998. Scaling Miscible Fluid Displacements in Porous Media. *Energy Fuels* **12**, 801–811. https://doi.org/10.1021/ef980020a

Hughes, T.J., Honari, A., Graham, B.F., Chauhan, A.S., Johns, M.L., May, E.F., 2012. CO2 sequestration for enhanced gas recovery: New measurements of supercritical CO2–CH4 dispersion in porous media and a review of recent research. *International Journal of Greenhouse Gas Control* **9**, 457–468. https://doi.org/10.1016/j.ijggc.2012.05.011

Jha, R.K., John, A.K., Bryant, S.L., Lake, L.W., 2009. Flow Reversal and Mixing. *SPE Journal* **14**, 41–49. https://doi.org/10.2118/103054-PA

John, A.K., 2008. Dispersion in Large Scale Permeable Media (*Ph.D. dissertation*). The University of Texas at Austin, Austin, Texas.

John, A.K., Lake, L.W., Bryant, S.L., Jennings, J.W., 2008. Investigation of Field Scale Dispersion, in: All Days. Presented at the SPE Symposium on Improved Oil Recovery, SPE, Tulsa, Oklahoma, USA, p. SPE-113429-MS. https://doi.org/10.2118/113429-MS

Lake, L., Johns, R.T., Rossen, W.R., Pope, G.A., 2014. Fundamentals of Enhanced Oil Recovery. *Society of Petroleum Engineers*. https://doi.org/10.2118/9781613993286

Lallemand-Barres, A., Peauclecerf, P., 1978. Recherche des relations entre Ie valeur de la dispersivite macroscopique d'un milieu aquifere, ses autres caracteristiques et les conditions de mesure. *Bull. Bur. Rech. Geol. Min*. **3**, 277–284.

Li, Y., Nghiem, L.X., 1986. Phase equilibria of oil, gas and water/brine mixtures from a cubic equation of state and henry's law. *Can J Chem Eng* **64**, 486–496. https://doi.org/10.1002/cjce.5450640319

Liu, S., Yuan, L., Zhao, C., Zhang, Y., Song, Y., 2022. A review of research on the dispersion process and CO2 enhanced natural gas recovery in depleted gas reservoir. *Journal of Petroleum Science and Engineering* **208**, 109682. https://doi.org/10.1016/j.petrol.2021.109682

Naudomsup, N., Lake, L.W., 2017. Extension of Capacitance-Resistance Model to Tracer Flow for Determining Reservoir Properties, in: Day 1 Mon, October 09, 2017. Presented at the SPE Annual Technical Conference and Exhibition, SPE, San Antonio, Texas, USA, p. D011S008R005. https://doi.org/10.2118/187410-MS

Oldenburg, C.M., Benson, S.M., 2002. CO2 Injection for Enhanced Gas Production and Carbon Sequestration, in: All Days. Presented at the SPE International Petroleum Conference and Exhibition in Mexico, SPE, Villahermosa, Mexico, p. SPE-74367-MS. https://doi.org/10.2118/74367-MS

Oldenburg, C.M., Pruess, K., Benson, S.M., 2001. Process Modeling of CO 2 Injection into Natural Gas Reservoirs for Carbon Sequestration and Enhanced Gas Recovery. *Energy Fuels* **15**, 293–298. https://doi.org/10.1021/ef000247h

Paul, G.W., Lake, L.W., Pope, G.A., Young, G.B., 1982. A Simplified Predictive Model for Micellar-Polymer Flooding, in: All Days. Presented at the SPE California Regional Meeting, SPE, San Francisco, California, p. SPE-10733-MS. https://doi.org/10.2118/10733-MS

Peaceman, D.W., 1977. Fundamentals of numerical reservoir simulation, Developments in petroleum science. Elsevier Scientific Pub. Co. # : distributors for the U.S. and Canadą Elsevier North-Holland, Amsterdam; New York.

Perkins, T.K., Johnston, O.C., 1963. A Review of Diffusion and Dispersion in Porous Media. *Society of Petroleum Engineers Journal* **3**, 70–84. https://doi.org/10.2118/480-PA

Peters, E.J., 2012. Advanced petrophysics. 1: Geology, porosity, absolute permeability, heterogeneity, and geostatistics. Live Oak, Austin, Tex.

Pooladi-Darvish, M., Hong, H., Theys, S., Stocker, R., Bachu, S., Dashtgard, S., 2008. CO2 Injection for Enhanced Gas Recovery and Geological Storage of CO2 in the Long Coulee Glauconite F Pool, Alberta, in: All Days. Presented at the SPE Annual Technical Conference and Exhibition, SPE, Denver, Colorado, USA, p. SPE-115789-MS. https://doi.org/10.2118/115789-MS

Schulze#Makuch, D., 2005. Longitudinal dispersivity data and implications for scaling behavior. *Groundwater* **43**, 443–456. https://doi.org/10.1111/j.1745-6584.2005.0051.x

Shook, M., Li, D., Lake, L., 1993. Scaling immiscible flow through permeable media by inspectional analysis. *International Journal of Rock Mechanics and Mining Sciences & Geomechanics Abstracts* **30**, A223. https://doi.org/10.1016/0148-9062(93)91860-L

Sigmund, P.M., 1976a. Prediction of Molecular Diffusion At Reservoir Conditions. Part II - Estimating the Effects Of Molecular Diffusion And Convective Mixing In Multicomponent Systems. *Journal of Canadian Petroleum Technology* **15**. https://doi.org/10.2118/76-03-07

Sigmund, P.M., 1976b. Prediction of Molecular Diffusion At Reservoir Conditions. Part 1- Measurement And Prediction of Binary Dense Gas Diffusion Coefficients. *Journal of Canadian Petroleum Technology* **15**. https://doi.org/10.2118/76-02-05

Van Der Meer, L.G.H., Kreft, E., Geel, C., Hartman, J., 2005. K12-B A Test Site for Co2 Storage and Enhanced Gas Recovery, in: All Days. Presented at the SPE Europec/EAGE Annual Conference, SPE, Madrid, Spain, p. SPE-94128-MS. https://doi.org/10.2118/94128-MS

Vandeweijer, V., Van Der Meer, B., Hofstee, C., Mulders, F., D'Hoore, D., Graven, H., 2011. Monitoring the CO2 injection site: K12-B. *Energy Procedia* **4**, 5471–5478. https://doi.org/10.1016/j.egypro.2011.02.532

Wang, W., Wen, J., Wang, C., Gomari, S.R., Xu, X., Zheng, S., Su, Y., Li, L., Hao, Y., Li, D., 2023. Current status and development trends of CO2 storage with enhanced natural gas recovery (CS-EGR). *Fuel* **349**, 128555. https://doi.org/10.1016/j.fuel.2023.128555